Air Entrainment Processes in a Circular Plunging Jet: Void-Fraction and Acoustic Measurements

H. Chanson
Reader,
Fluid Mechanics, Hydraulics and Environmental Engineering,
Department of Civil Engineering,
The University of Queensland,
Brisbane QLD 4072, Australia
e-mail: h.chanson@uq.edu.au

R. Manasseh
Senior Research Scientist,
CSIRO Thermal and Fluid Engineering,
P.O. Box 56,
Highett VIC 3190, Australia
e-mail: richard.manasseh@dbce.csiro.au

Circular plunging jets were studied by both void fraction and acoustic techniques. There were two aims: to measure the structure of the jet flow and its regimes as a function of jet speed and free-jet length; and to develop and validate the acoustic measurement technique in the developing flow. Void fractions and bubble count rates were measured in the developing shear layer of a large-size plunging jet ($d_1 = 25$ mm). The data compared well with a solution of an advective diffusion equation and showed an increased air entrainment rate with increasing free-jet length for $x_1/d_1 \leqslant 12$. The acoustic data were processed by a novel technique to extract both bubble count and bubble size data. Three plunging jet flow regimes were noted. Near inception, acoustic pulses are isolated and indicate individual bubble entrainment as observable visually. Above a characteristic jet velocity, the number of the bubble pulses increases sharply although bubbles are still produced intermittently. At higher velocities, bubble production becomes quasi-continuous. The study suggests that an acoustic technique calibrated through detailed laboratory measurements can provide useful, absolute data in high-void fraction flows. The robust acoustic sensor can then be used in hostile industrial or environmental flows where more delicate instruments are impractical. [DOI: 10.1115/1.1595672]

Introduction

Plunging jet entrainment is a highly efficient mechanism for producing large gas-liquid interfacial areas. Applications include minerals-processing flotation cells, waste-water treatment, oxygenation of mammalian-cell bioreactors, riverine re-oxygenation weirs and the understanding of plunging ocean breakers, [1–3]. While detailed air-water flow measurements were conducted in a two-dimensional plunging jet, [4–6], most studies of air entrainment processes at circular plunging jets have been qualitative (Table 1, [2,7,8]). It is understood that plunging jet entrainment takes place when the jet impact velocity exceeds a critical velocity, [9,10]. For larger jet velocities, the developing region of plunging jet flow is subjected to strong interactions between the entrained air bubbles and the momentum transfer mechanism, [11].

While intrusive probe measurements (e.g., conductivity and optical probes that pierce the bubble) give local flow properties including void fraction and bubble count rate, the acoustic technique may provide useful information on the bubble size distribution, the onset of bubble entrainment and the entrainment regime. Bubbles generate sounds upon formation and deformation, [12,13], that are responsible for most of the noise created by a plunging jet. Most underwater acoustic sensors are made from robust piezoelectric crystals and a key advantage is their robustness for use in the field and in hostile environments.

This study is based upon a comparison of conductivity probe and acoustic measurements in the developing flow region of a large plunging jet system. Although the present acoustic technique was originally calibrated against precision laboratory photographs of rapidly produced bubbles, [14], comparisons with intrusive measurement techniques are limited. Furthermore, there are serious questions in interpreting acoustic signals when void fractions are high or bubbles form a fine cloud, [15]. The present work takes further steps towards an acoustic signature technique for characterizing the performance of a bubbly flow system with large void fractions in which both acoustics and intrusive properties of a bubbly shear flow are accurately documented.

Experimental Apparatus and Methods

The experimental apparatus (Fig. 1) consisted of a fresh water circular jet issuing from a 0.025 m diameter nozzle. The receiving channel was 0.3 m wide and 1.8 m deep with glass side walls 10 mm thick. The nozzle was made of aluminum with a 1/2.16 contraction ratio designed with an elliptical profile. Upstream of the nozzle, water was supplied by a straight circular pipe (0.054 m internal diameter, 3.5 m long). The jet and pipe were vertical to within ± 0.5 deg. The water supply (Brisbane tap water) was provided by a constant-head tank with a water level about 12.9 m above the nozzle. The apparatus provided nozzle velocities between 0.3 and 7 m/s. Further information were presented by Manasseh and Chanson [16].

Instrumentation. The discharge was measured with an orifice meter (British Standards design) calibrated on-site with a volume-per-time technique. The error on the discharge measurement was less than 1%.

All measurements were taken on the jet diameter through the centerline. The displacement of the probes in the flow direction and in the direction normal to the jet centerline was controlled by fine adjustment travelling mechanisms and measured with two Lucas Schaevitz Magnarules Plus MRU-012 and MRU-036. The error in the probe position was less than 0.1 mm in each direction.

In the free-falling jet, clear water jet velocities and turbulent velocity fluctuations were measured using a Prandtl-Pitot tube (diameter 3.3 mm) and a conical hot-film probe system. The Prandtl-Pitot tube was connected to a Validyne pressure transducer scanned at 500 Hz. The miniature hot-film probe (Dantec 55R42, 0.3 mm size) was scanned at 40 kHz. It was initially calibrated

Contributed by the Fluids Engineering Division for publication in the JOURNAL OF FLUIDS ENGINEERING. Manuscript received by the Fluids Engineering Division Oct. 16, 2001; revised manuscript received Mar. 10, 2003. Associate Editor: L. Mondy.

Table 1 Experimental flow conditions of circular vertical plunging jets. x_1: longitudinal distance between the nozzle and the free-surface pool; Tu_1: jet turbulence intensity at impact; Tu_o: turbulent intensity measured at jet nozzle; (—): information not available; N/a: not applicable.

Ref. (1)	Run (2)	x_1 m (3)	V_1 m/s (4)	d_1 m (5)	Tu_1 (6)	Comments (7)
Lin and Donelly [40]		0.020	0.8 to 2.04	0.002 to 0.008	—	Liquids: water, oil, glycol
Ervine et al. [9]		up to 5	0.8 to 9	—	—	$d_o=0.006$ to 0.025 m. $Tu_o=0.3$ to 8%
McKeogh and Ervine [29]		—	2.5 to 3.3	0.009	—	Fig. 6 ($Tu_o=5\%$), Fig. 8 ($Tu_o=1\%$) & Fig. 9 ($Tu_o=1\%$)
Van de Donk [41]		0.20	4.47 to 10.2	0.0057	—	Fig. 3.22 and 3.23
Detsch and Sharma [28]		—	1 to 7	—	—	$d_o=0.0015$ to 0.002 m. Liquids; water, salt water, ethanol, ethylene glycol solutions
Bonetto and Lahey [27]		0.01 and 0.03	5.3 to 7.9	0.0051	—	Figs. 11, 13, and 16
Elhammoumi [21]		0.29	3.1 and 3.7	0.0073 & 0.012	—	$Tu_o=0.0001$ to 0.0028%
Present study						$d_o=0.025$ m. Tap water ($\sigma=0.055$ N/m).
	BM013	0.005	0.52	0.0224	0.012	Onset of air bubble entrainment
	BM08	0.023	0.87	0.0200	0.0098	Onset of air bubble entrainment
	BM09a	0.10	1.58	0.0171	0.0047	Onset of air bubble entrainment
	BM09b	0.20	2.10	0.0145	0.004	Onset of air bubble entrainment
	BM03	0.02	1.27 to 5.85	N/a	N/a	Observations of bubble penetration depth
	BM01	0.1	1.68 to 5.01	N/a	N/a	Observations of bubble penetration depth
	BM04	0.2	2.24 to 5.85	N/a	N/a	Observations of bubble penetration depth
	RM3	0.005	0.94 to 5.0	N/a	N/a	Acoustic measurements. Hydrophone location: $r/d_1=0.5$ & 1.5, $x-x_1=0.02$ & 0.05 m.
	RM1	0.02	5.0	—	0.0035	Acoustic measurements. Hydrophone location: $r/d_1=0.5$ & 1.5, $x-x_1=0.02$ & 0.05 m.
	RM12	0.1	1.69 to 4.32	N/a	N/a	Acoustic measurements. Hydrophone location: $r/d_1=0.5$, $x-x_1=0.02$ m.
	RM20	0.3	4.57 to 4.75	N/a	N/a	Acoustic measurements. Hydrophone location: $r/d_1=0.5$, $x-x_1=0.02$ m.
	BM31_1	0.005	3.1	0.0249	0.0034	Resistivity probe measurements
	BM4_1	0.005	3.9	0.0250	0.0034	
	BM44_1	0.005	4.4	0.0250	0.0031	
	BM5_1	0.005	4.96	0.0250	0.0032	
	BM5_2	0.02	4.99	0.0249	0.0035	
	BM35_1	0.1	3.5	0.0239	0.0039	
	BM4_2	0.1	4.1	0.0242	0.0046	
	BM44_2	0.1	4.4	0.0243	0.0095	
	JV5	0.1	5	0.02455	0.0095	
	JV6	0.1	6	0.0247	—	
	BM5_3	0.2	4.986323	0.0240	0.0079	

with the Pitot tube data and the velocity distribution was checked with the measured flow rate (within 2%) for jet velocities ranging from 1 to 5 m/s.

A single-tip resistivity probe (inner electrode 0.35 mm and outer electrode 1.42 mm) was used to measure void fraction and bubble count rates in the plunging jet flow. The probe was excited by an air bubble detector (Ref. AS25240) with a response time less than 10 μs. Measurements were recorded with a scan rate of 5 kHz for 180 s.

Underwater acoustics were measured with a hydrophone (Brüel and Kjær type 8103) connected to a charge amplifier (Brüel and Kjær type 2635). The hydrophone was located at $r/d_1=0.5$ and $x-x_1=0.02$ m for most experiments (Table 1, column 7), where r is the radial distance measured from the jet centerline, d_1 is the jet diameter at impact, x is the longitudinal distance, and x_1 is the free jet length (Fig. 1(*a*)). A digital audio tape (DAT) recorder (Sony TCD-D7) digitized the signal at 44.1 kHz, implying an alias frequency of about 22 kHz. The range of jet conditions caused a difference in acoustic signal power of up to 20 dB (a factor of 10 in amplitude) between experiments. Since all data recorded on tape should have similar magnitudes to avoid distortion or loss of dynamic range, the charge amplification was set for each experiment to deliver optimal recorded quality and corrected for during the signal processing. DAT recordings were processed with a HP35670A dynamic signal analyzer. Fast Fourier transforms (FFTs) were taken. Each experimental dataset was subsampled into 500 sets 15.6 ms long to give a frequency span of 0–25.6 kHz. The data were also processed by a bubble-acoustic software StreamTone, [17].

Experimental Errors. The error on the void fraction C was estimated as $\Delta C/C\sim 3\%$ for $C\geqslant 5\%$ and $\Delta C/C\sim 0.5\%/C$ for $C\leqslant 5\%$. The minimum detectable bubble chord length is about 0.3 mm with the resistivity probe and also with the acoustic analysis. The accuracy of clear-water velocity V was about $\Delta V/V=1\%$. For the acoustic data, 95% confidence limits were calculated for the averaged spectrum for each run. At low speeds ($V_1<2.5$ m/s where V_1 is the jet velocity at impact), the acoustic signal was very intermittent. Although the representativity of these runs could not be checked, their averaged spectrum appeared statistically stationary within 500 samples. At higher speeds, statistical stationarity was easily obtained within 500 samples, while the StreamTone software gave an error in repeatability of less than 1% on bubble size, which was less than the 95% statistical confidence interval on the mean.

Experimental Flow Conditions. The flow conditions are summarized in Table 1, showing the flow rate Q_w, the free-jet

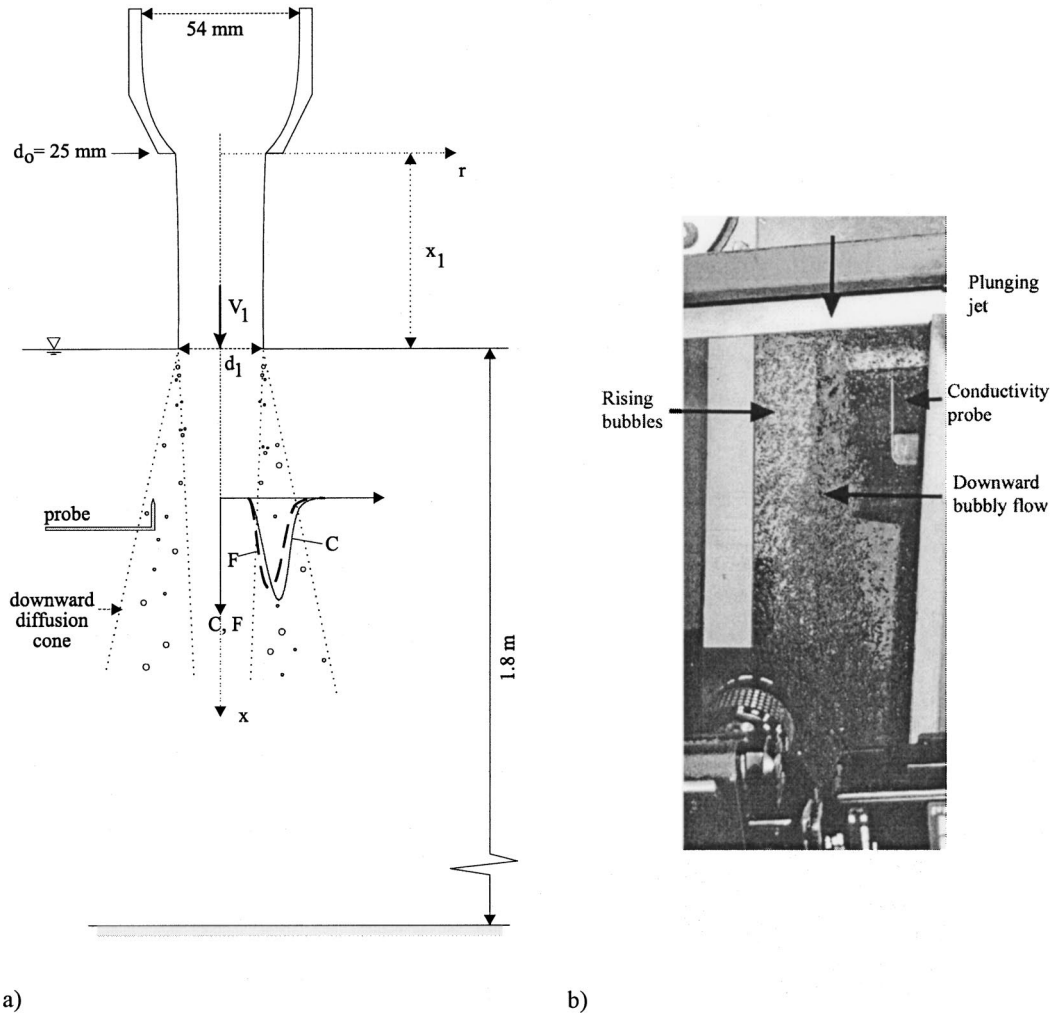

Fig. 1 Vertical circular plunging jet apparatus. (*a*) Sketch of the apparatus, (*b*) high-speed photograph for V_1=3.3 m/s, x_1=0.1 m.

length x_1, the impact flow velocity V_1, and diameter d_1. For each test, the water jet was extremely smooth and transparent. No air entrainment was visible upstream of the impingement point. Velocity and velocity fluctuation distributions, performed 5 mm downstream of the jet nozzle, were uniform for nozzle velocities ranging from 0.5 to 5 m/s. In the present study, the free-jet lengths ranged from 0.005 up to 0.3 m, and the impingement velocities were between 0.5 and 6 m/s.

The turbulence intensity of the water jet core was measured on the centerline at the impingement point. The data suggest that the turbulence level decreased with increasing jet speed for a given jet length (Table 1, column 6). For a constant plunge velocity, the turbulence increased gradually with the free-jet length for $0.2 \leqslant x_1/d_1 \leqslant 8$.

Physical Modeling and Scale Effects. In a physical model, the flow conditions are said to be similar to those in the prototype if the model displays similarity of form, similarity of motion, and similarity of forces. Dynamic similarity of plunging jet flows is, however, complex because of a variety of factors such as flow aeration, interactions between entrained bubbles and developing mixing layer, and others. In a geometrically similar model, true dynamic similarity is achieved only and only if each dimensionless parameter (or Π-terms) has the same value in both model and prototype. For example, for small facilities, bubble entrainment is strongly dependent on the scale of the experiment, [2,18,19]. For civil and environmental engineering applications, the latter recommended the use of model scales ranging from 10/1 to 1/10 to avoid significant scale effects, [2]. Conversely experimental results obtained in a large size facility cannot be down-scaled. In the context of this study, a large-size plunging jet facility (d_1 = 25 mm, pool depth: 1.8 m) was used to minimize scale effects when the results are upscaled to larger industrial facilities.

Air Bubble Entrainment Regimes

In a plunging jet, air bubbles start to be entrained when the jet impact speed V_1 exceeds a critical value. McKeogh [20] showed that the inception speed decreases with increasing jet turbulence for a given jet configuration.

In the present study, inception of bubble entrainment is defined as the threshold at which one bubble is entrained during a 3-minute period. Results are presented in Tables 1 and 2. Air bubble entrainment was detected visually and photographically for V_1 between 0.55 and 2.1 m/s while acoustic measurements were made up to 5.0 m/s. The data show that the inception velocity increases with increasing free-jet height x_1 which corresponds to a decrease in jet turbulence intensity (Table 1). The result is consistent with previous observations, [9,10,21], although it does not follow a conceptual model of increased free-jet surface roughness, [22,23].

For $V_1 > 0.7$ m/s, visual and photographic observations suggest three entrainment regimes, summarized in Table 2. In Regime I (i.e., for impact speeds slightly greater than the inception speed),

Table 2 Characteristic jet impact velocity V_1 (m/s) for the transitions between three entrainment regimes

x_1 (m) (1)	Inception (2)	V_1 (m/s) RI–RII (3)	RII–RIII (4)
0.005	0.52	1.0	3.5–5
0.023	0.87	—	—
0.10	1.58	1.7	2.5
0.20	2.10	—	—

fine individual bubbles are irregularly entrapped. The time interval between successive entrapment events may reach up to few minutes, as previously observed by Cummings and Chanson [10] for a plane jet. The entrapment process is distinctly audible using the hydrophone. Although some bubble trajectories are vertical, most entrained bubbles tend to follow a slightly helicoidal trajectory, consistent with previous studies, [24–26]. Note that void fraction measurements were inaccurate in Regime I because the void fraction was less than 0.1%.

With an impact speed of about 1.0 m/s for $x_1=5$ mm, an unstable air cavity starts to develop at one point along the impingement perimeter (Regime II). The air cavity position changes with time in an apparently random manner. Larger air packets are entrained below the air cavity with the stretching and breakup of the cavity tip.

At larger speeds (above about $V_1=3.5$ to 5 m/s for $x_1=5$ mm), the air cavity develops all around the perimeter and most air is entrained by elongation, stretching and breakup of the ventilated cavity (Regime III). Bonetto and Lahey [27], Cummings and Chanson [4], and Chanson and Brattberg [11] elaborated on this regime. Visually most entrained air bubbles/packets tend to follow a somewhat helicoidal trajectory. The rotation direction fluctuates irregularly at a low frequency (less than 0.5 Hz). Similar bubble trajectory rotation fluctuations were studied in detail by Yoshida et al. [25]. Furthermore, the direction seems related to the rotation sense of the free-surface vortex. Detsch and Sharma [28] reported a similar effect. Regime III is common in industrial processes.

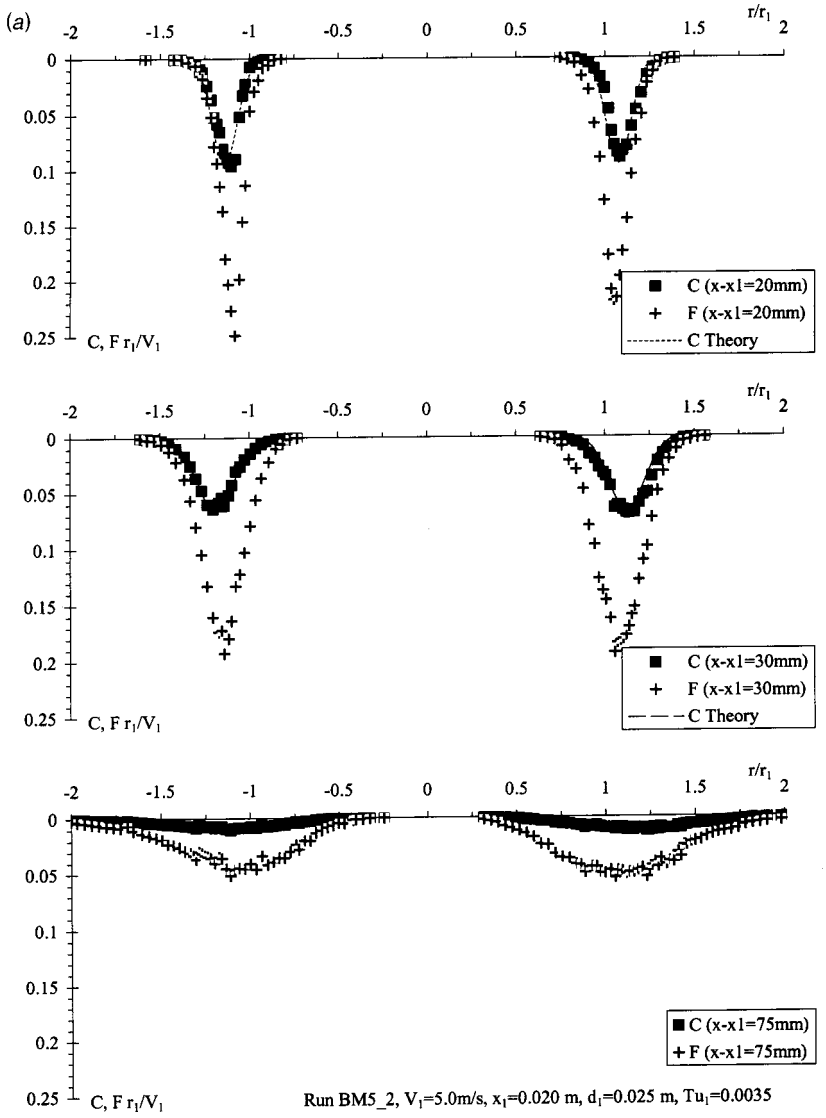

Fig. 2 Dimensionless distributions of void-fraction and bubble count. Dashed line is solution of Eq. (1). Tu_1 is turbulence intensity based on longitudinal velocity fluctuations at jet impact. *(a)* **Jet height, $x_1=20$ mm, jet velocity $V_1=5.0$ m/s, $Tu_1=0.35\%$.** *(b)* **Jet height $x_1=100$ mm, jet velocity $V_1=3.5$ m/s, $Tu_1=0.39\%$.**

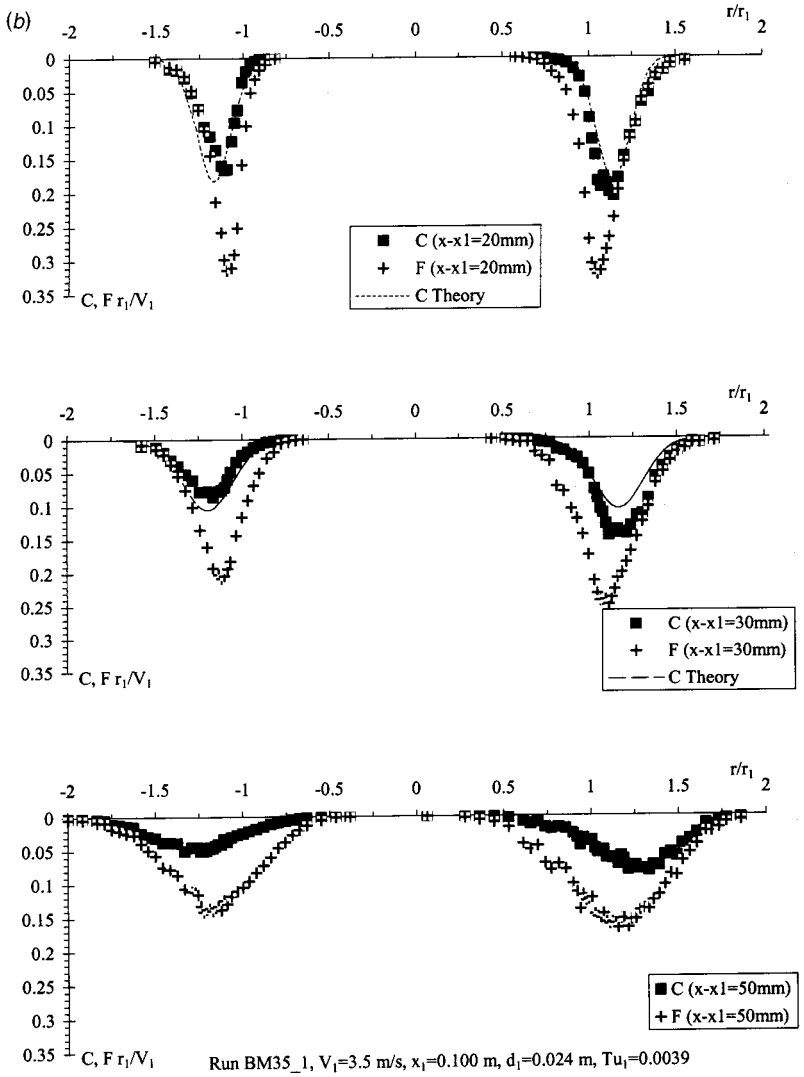

Fig. 2 (***continued***)

Spatial Distributions of Void Fraction and Bubble Count Rate

Void-fraction measurements show the advective dispersion of the entrained air bubbles in the developing flow region. Void fraction and bubble count rate data are presented in Fig. 2, for two impact flow velocities ($V_1=5.0$ and 3.5 ms) and free-jet lengths ($x_1=0.02$ and 0.1 m, respectively). Results for other velocities and free-jet lengths show similar curves and can be found in Manasseh and Chanson [16].

The distributions of void fraction are consistent with the earlier studies by McKeogh and Ervine [29] and Bonetto and Lahey [27] with 9 mm and 5.1 mm circular jets, respectively. The data compare favorably with a simple analytical solution of the advective diffusion solution,

$$C=\frac{Q_{\text{air}}}{Q_w}\frac{1}{8D^{\#}X}\exp\left(-\frac{R^2+1}{8D^{\#}X}\right)I_o\left(\frac{R}{4D^{\#}X}\right), \qquad (1)$$

where Q_{air} is the quantity of entrained air, Q_w is the water jet flow rate, $D^{\#}=2\,D_t/(V_1 d_1)$, D_t is the advective diffusion coefficient, $X=(x-x_1)/d_1$, $R=2\,r/d_1$, x is the distance along the flow direction measured from the jet nozzle, r is the radial distance from the jet centerline, and I_o is the modified Bessel function of the first kind of order zero, [2]. For each run, the values of Q_{air}/Q_w and $D^{\#}$ were determined from the best fit of the data to Eq. (1). Note that the data were best fitted by assuming $R=2\,(r+\delta r)/d_1$ where $\delta r>0$ increases with increasing distance x for a given experiment. For very low entrainments rates (e.g., Fig. 6(*a*)), void fraction distributions exhibited some dissymmetry which might be attributed to a feedback mechanism between the probe and developing vortices. It is hypothesized that the probe support interfered with the developing shear region, preventing the development of helicoidal vortical structures. In turn air entrapment was affected and found to be lesser on one side or another.

Bubble count rates were also measured at each point. Typical distributions are shown in Fig. 2. For a given void fraction and velocity, the bubble count rate is inversely proportional to the bubble diameter and proportional to the specific interfacial area, [30,31]. It provides additional information on the bubbly flow structure.

In the developing flow region, the void fraction distribution exhibits a peak ($C=C_{\max}$) at $r=r_{C_{\max}}$ at a given cross section (x constant). The distributions of bubble count rate F also show a maximum ($F=F_{\max}$) in the developing flow region, but at $r=r_{F_{\max}}$, where $r_{C_{\max}}$ and $r_{F_{\max}}$ are significantly different. For $(x-x_1)/d_1<8$ and all jet lengths, the bubble count peak was consistently on the inside of the void-fraction peak: i.e., $r_{F_{\max}}<r_{C_{\max}}$. The result is consistent with the observations of Brattberg and Chanson [6] for a plane jet.

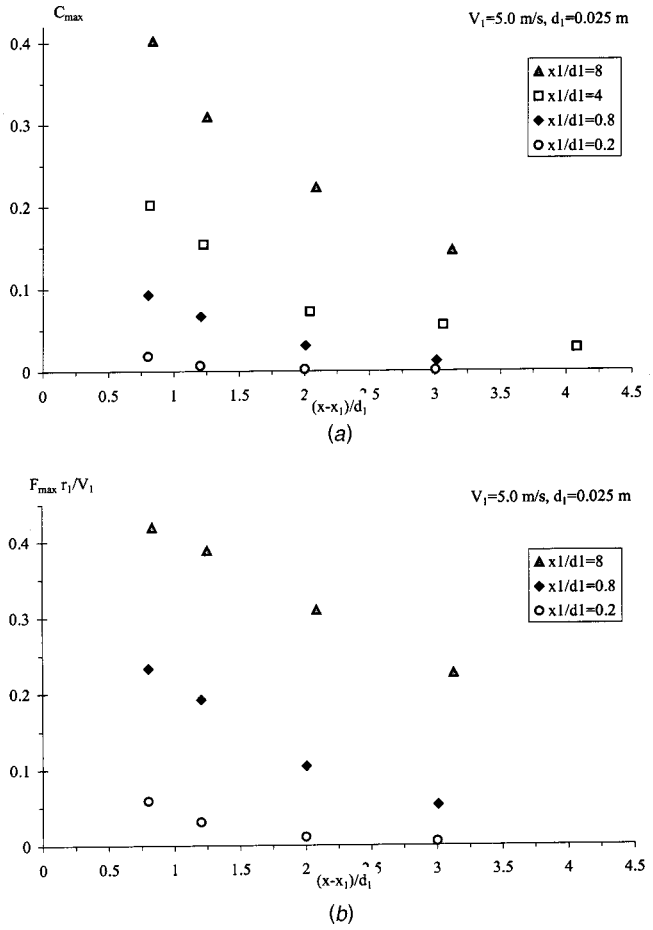

Fig. 3 Effect of the free jet length on the maximum void-fraction and bubble count. (*a*) Maximum void fraction, (*b*) maximum dimensionless bubble count.

Figure 3 illustrates the effect of the free-jet length x_1 on the maximum void fraction and bubble count. The data were recorded for an identical impact velocity V_1 at several vertical depths. The results show that the air entrainment rate increases with increasing jet length. It is proposed that short jet lengths (e.g., $x_1/d_1<0.2$ to 0.8) prohibit the development of large vortical structures with scale comparable to the jet diameter, hence preventing the development of free-jet turbulence favorable to bubble entrainment at the plunge point. For long free-jets, Van de Sande and Smith [32] suggested that interfacial aeration of the free-jet may contribute significantly to an increase in air entrapment. During the present study, the free-jet was visually transparent for $x_1/d_1<40$ and all investigated jet velocities.

Although the maximum void fraction and count rate become small for $(x-x_1)/d_1>5$ to 7 (Fig. 3), individual bubbles were seen at much greater depths (Fig. 1(*b*)). Millimetric bubbles were seen at depths of $(x-x_1)/d_1=30$ to 75 for free-jet lengths x_1 increasing from 5 to 200 mm, respectively. For the longest jet length, the observation was close to the results of Clanet and Lasheras [33]. However, fine bubbles (sizes less than 0.5 to 1 mm) were consistently observed at deeper depths for impact velocities greater than the onset velocity. Visual observations showed that tiny bubbles could be trapped in large vortical structures for several minutes, before being ejected to another vortical structure or toward the free surface. Some bubbles could stay near the flume bottom more than five minutes.

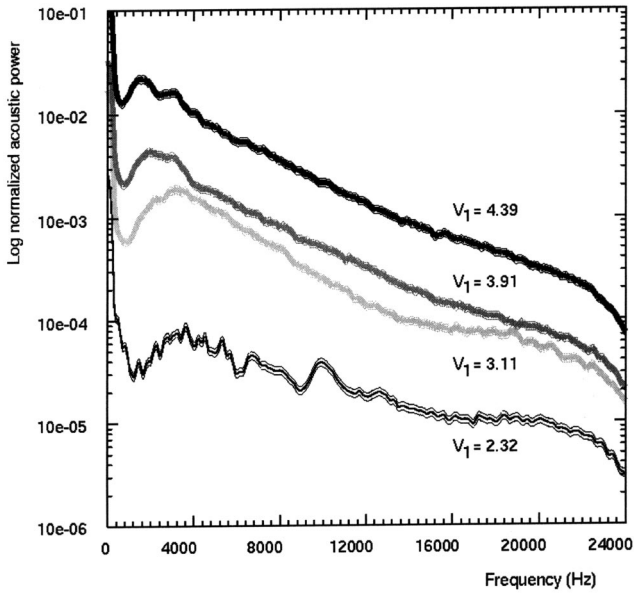

Fig. 4 Acoustic spectra, jet height $x_1=5$ mm after [16]

Acoustic Analysis of Entrainment Regimes

Acoustic Spectrum and Bubble Size Measurements. The acoustic data were analyzed following principles detailed elsewhere, [13,17]. Two techniques were used: a continuous, spectral analysis following Pandit et al. [34], and a discrete, pulse-wise analysis following the ''first-period'' method of Manasseh et al. [17]. The spectral analysis utilizes all bands of the signal, offering an overall ''signature'' of the system. However, the conversion to bubble-size spectra relies on a questionable assumption: that bubbles of different sizes are perturbed to the same proportional extent. The pulse-wise analysis can give greater accuracy on the true bubble frequencies, and offers the benefit of bubble count-rates, giving the Sauter-mean diameter of practical interest. However, in correcting the pulse-wise distributions to account for the greater amplitude of large bubbles, exactly the same questionable

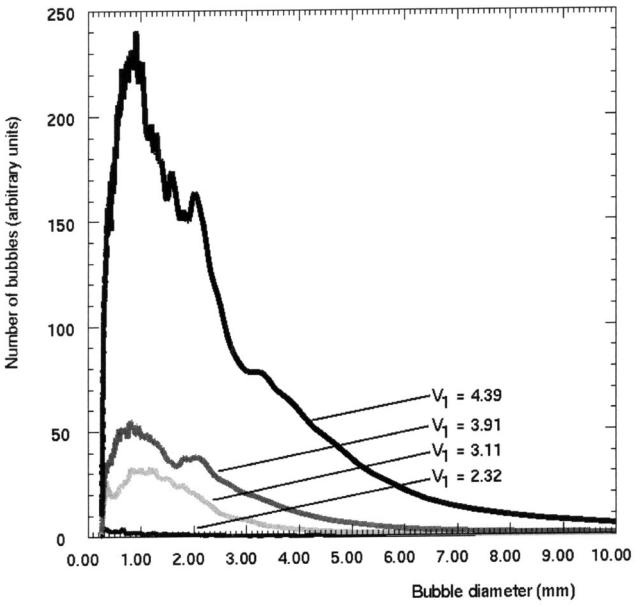

Fig. 5 Bubble-size spectra, jet height $x_1=5$ mm after [16]

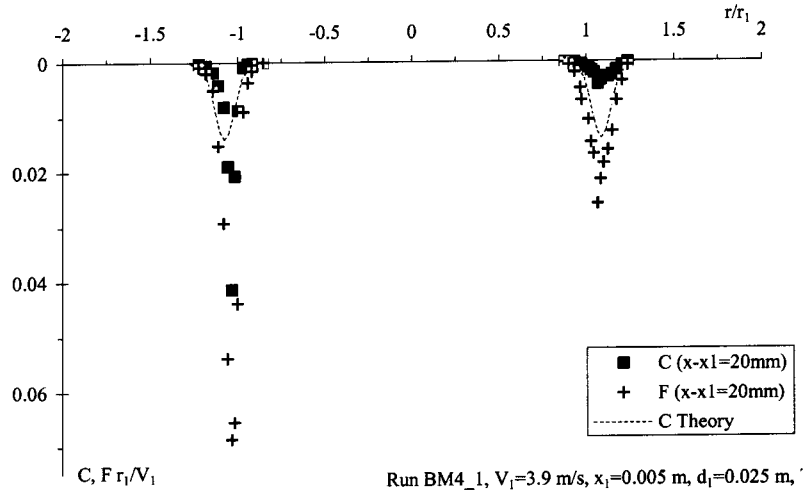

(*a*)

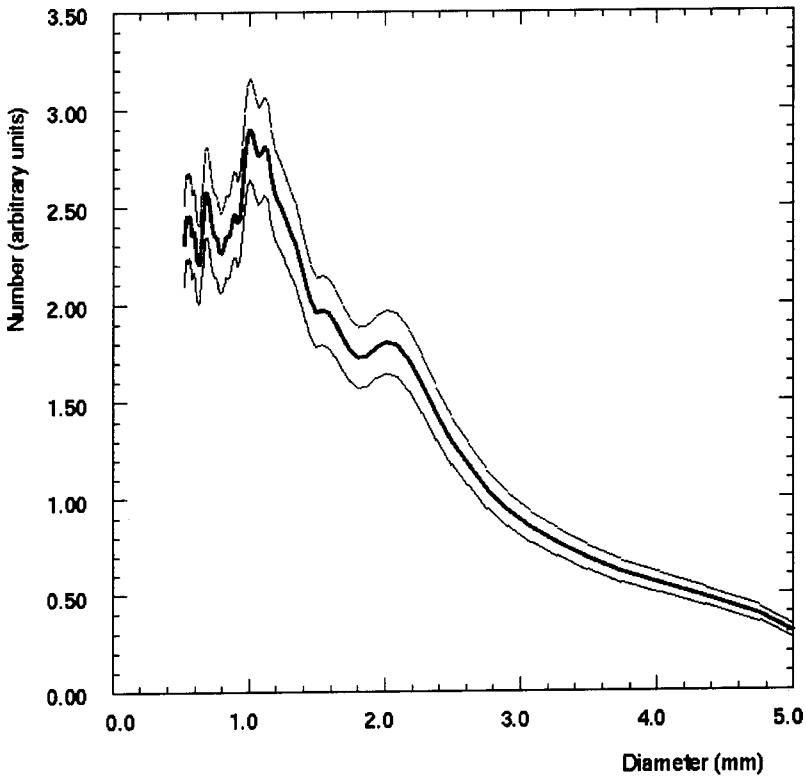

(*b*)

Fig. 6 Void-fraction, bubble count, and detailed bubble size spectrum, jet height $x_1 = 5$ mm, speed $V_1 = 3.9$ m/s. Dashed line in (*a*) is solution of Eq. (1). Tu_1 is turbulence intensity based on longitudinal velocity fluctuations; (*b*) after [16].

assumption on bubble excitation must be made. Both techniques also assume the bubble do not interact acoustically. Aspects of the techniques relevant to the present study are detailed in the Appendix.

Typical acoustic spectra are shown in Fig. 4 for the same geometric conditions ($x_1 = 0.005$ m, $x - x_1 = 0.020$ m, $d_1 = 0.025$ m) as in Fig. 6(*a*), and for several jet velocities. Each spectrum was normalized to its integral. Since different amplifications were used for some experiments, the normalized spectra were shifted in the vertical to account for the amplification used during each experiment, ensuring that comparisons between experiments with different amplifications were valid.

In Fig. 4, the ordinate is a logarithmic scale and fine lines bracketing the central lines indicate the bounds of 95% statistical confidence intervals. High-velocity experiments exhibit higher acoustic energy, illustrating a louder underwater noise. Each spectrum shows a minimum in energy at roughly 400 Hz, indicating that low-frequency noise probably due to background turbulence is below 400 Hz. In Regime II (e.g., $V_1 = 2.32$ m/s), individual bubble signals were very clear to the ear (in other words, a time series of the sound would show a series of clearly separated pulses); and a broad peak was centered around $f = 3.6$ kHz. Such a frequency corresponds to bubbles around 1.8 mm in diameter (Appendix Eq. (4)). With increasing jet speed, the frequency peak

shifted to lower frequencies. For the highest jet speed in Regime III, (i.e., $V_1=4.4$ m/s, Fig. 4), the peak was at about $f=1.7$ kHz, corresponding to bubbles about 3.8 mm in diameter. Since all peak frequencies were greater than the low-frequency noise found below 400 Hz, no high-pass filtering was required.

The bubble-size spectra may be derived from the acoustic spectra. Figure 5 presents the bubble-size spectra for the acoustic data shown in Fig. 4. (Figure 6(*b*) shows one of the curves of Fig. 5, for $V_1=3.9$ m/s, in better detail.) A major difference is the large number of bubbles in Regime III ($V_1=4.4$ m/s). For all acoustic experiments, the bubble-size spectra show a distinctive peak in the production of bubbles around 1 mm in diameter. Chord-length data for related two-dimensional flows showed also a peak around 1 mm, [5]. The aliasing frequency of the equipment of 22 kHz implies a cutoff to bubbles below 0.3 mm in diameter. Since the peaks in Fig. 4 fall off well before 0.3 mm, it is believed that they are genuine peaks subject only to the uncertainties of the assumptions in the analysis.

In Fig. 5, there is a second peak around 2.0 mm diameter for the larger-velocity data (i.e., $V_1=4.4$ and 3.9 m/s), while there is a smaller but significant third peak at about 1.6 mm in the $V_1=4.4$ m/s data. The corresponding ratio 2.0/1.6 is about the cube root of two. It could be inferred that, in Regime III, pairs of 1.6 mm bubbles are coalescing to form 2.0 mm bubbles, or alternatively that 2.0 mm bubbles are breaking up, [10,35]. However Cummings and Chanson [35] never observed bubble coalescence for $x-x_1<0.2$ m in a planar plunging jet. Both video and still photographs highlighted breakage only. Figure 6 shows acoustic and void-fraction data for one experiment: that is, $V_1=3.9$ m/s (Regime III). The resistivity probe data are shown in Fig. 6(*a*) while acoustic data are shown with 95% statistical confidence intervals in Fig. 6(*b*).

The spectral method of measuring bubble size has a number of disadvantages, [17]. Among these is the absence of data on bubble counts, readily provided by the resistivity probe. A quantity of practical interest to chemical engineers is the Sauter mean diameter:

$$D_{32}=\frac{\Sigma_{i=1}^{n}D_i^3}{\Sigma_{i=1}^{n}D_i^2} \tag{2}$$

where D_i is the diameter of a bubble and n is the total number of bubbles detected. In industry, D_{32} has traditionally been calculated by sampling individual bubbles and measuring them optically. A technique based on measurements of individual bubbles, rather than overall spectra, would be compatible with industrial experience, since it would enable the Sauter-mean diameter to be calculated and compared with optical measurements where those are available. Manasseh et al. [17] proposed an alternative ''first-period'' method providing the distribution of bubble sizes based on the identification of individual bubble pulses. The data can be used to infer bubble count rates and the Sauter mean diameter as well as a size distribution (Appendix).

The acoustic bubble count rate was calibrated based upon the count rates measured by the resistivity probe for identical flow conditions. The similar cutoff bubble size of 0.3 mm may help to match the two techniques. A typical distribution is shown in Fig. 7; its features are reproducible in multiple samples of data from the same settings. The trigger levels were scaled by the amplification used during each experiment. The location of the peaks in the corrected distributions (e.g., Fig. 7) are consistent with the frequency spectra (e.g., Fig. 6). (The distribution cuts off below 0.5 mm and above 3.3 mm owing to the windowing process by which the pulses were processed.) Figure 7, however, provides more details which may stem from the greater accuracy of the first-period method, [14]. The peak around 1 mm is in fact a double peak with subpeaks at 0.80 and 1.04 mm. Since the ratio of these sizes is close to the cube root of two, there may be a tendency for the 1.04 mm bubbles to split into two equal daughter bubbles, [10,35].

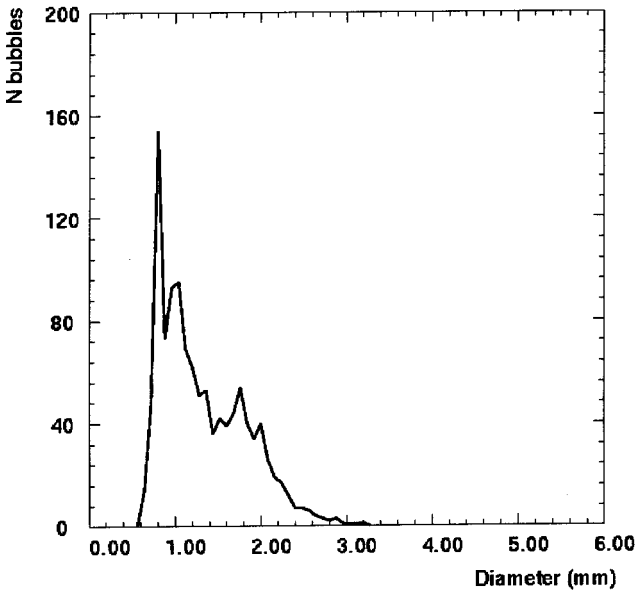

Fig. 7 Bubble-size distribution, jet height $x_1=5$ mm, speed $V_1=3.9$ m/s (acoustic data after [16])

The variations of bubble count rate F, mean corrected bubble size D_1, and Sauter mean diameter D_{32} are shown in Fig. 8 as functions of the jet velocity at impact. Each acoustic data point is based on the analysis of four minutes of data. The vertical error bars represent 95% statistical confidence intervals on the acoustic measurement. The bubble count rate data highlight the transition from Regime II to Regime III, with a sudden increase in bubble production (i.e., bubble count rate) at around $V_1=2.5$ m/s. This is heard as a change from individual ''plinking'' sounds to a ''rushing'' sound. The bubble count rate appears to be maximum around $V_1=3$ m/s (Fig. 8).

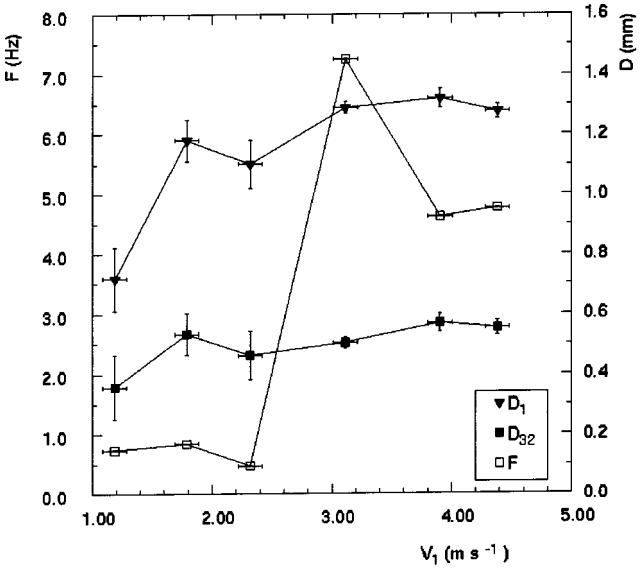

Fig. 8 Bubble count rates and diameters as a function of jet speed V_1, jet height $x_1=5$ mm (acoustic data)

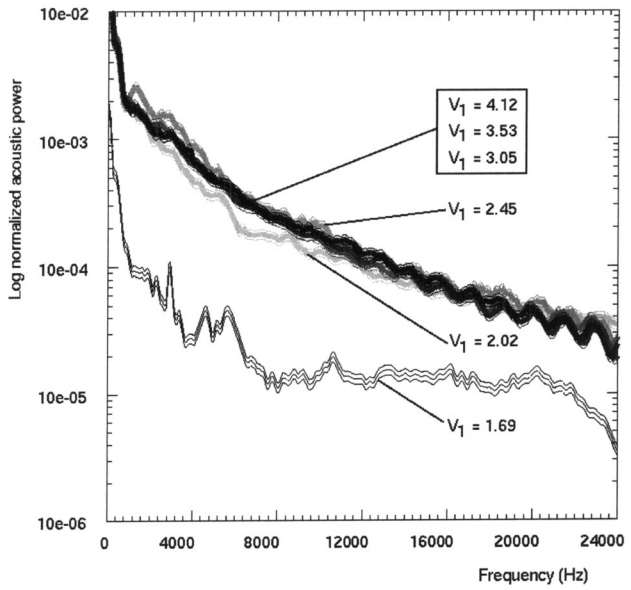

Fig. 9 Acoustic spectra, jet height $x_1 = 100$ mm

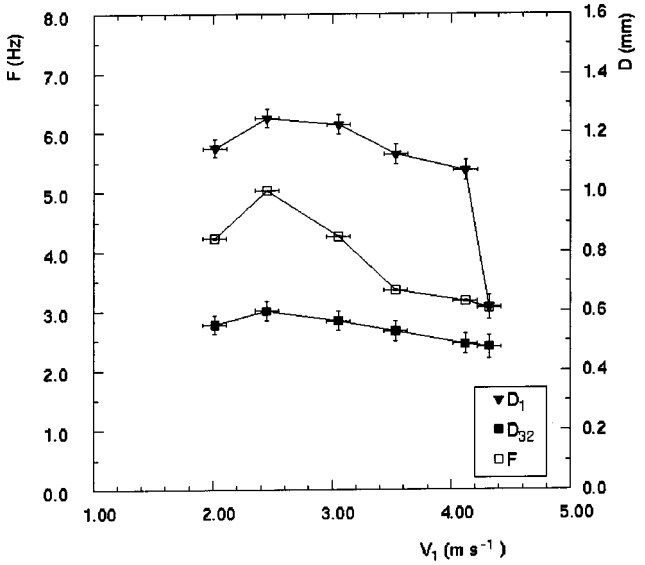

Fig. 11 Bubble count rates and diameters as a function of jet speed V_1, jet height $x_1 = 100$ mm

Effect of Jet Height on Acoustic Data. The above results were focused on experiments with a constant jet height x_1. Figure 9 presents data for a larger jet height of $x_1 = 0.1$ m. The data show that Regime II occurs at a lower jet velocity V_1 compared to the experiments with $x_1 = 0.005$ m (Table 2). The spectrum in Regime II has significantly less power than the spectra in Regime III (e.g., $V_1 = 3.9$ m/s) simply reflecting the fact that bubbles are not produced continually.

Although the boundary between Regime II and Regime III is detectable by ear between 2.0 and 2.4 m/s, there is little significant difference in the spectra for $V_1 > 2$ m/s. This is a marked contrast to the spectra for $x_1 = 0.005$ m, when increasing V_1 above the inception condition continues to increase the total sound power produced. The spectra also decay relatively monotonically.

In Fig. 9, there is some high-frequency noise in the system above about 14 kHz, the source of which is unknown. There might be aliased high-frequency energy in the data. It may be that, with the higher jet height of 100 mm, the bubble-size distribution becomes fixed (''saturated'') at a lower jet velocity. If this is the case, the effect of increasing the jet height is to decrease the importance of variations in the jet speed V_1, at least as far as the bubble-size distribution is concerned (Fig. 10). The bubble count rate F, mean corrected bubble size D_1 and Sauter-mean diameter D_{32} show a similar lessening of the importance of V_1 (Fig. 11): The sudden jumps in the curves at the low jet height no longer occur, since the transition from one regime to the next is not so marked at the high jet height.

The software measuring the bubble count rate based upon acoustic data can process up to 20 bubbles per second. It is unlikely that the maximum around six counts per second represents a saturation of the measurement system. An identical analysis protocol was used for each impact velocity V_1, with the straightforward correction for different amplifications during recording being the only variation. Since increasing the jet speed at a given height demands greater pumping costs, these results suggest that as long as the jet height exceeds a threshold, the jet speed could be fixed at a low level for the same aeration benefit.

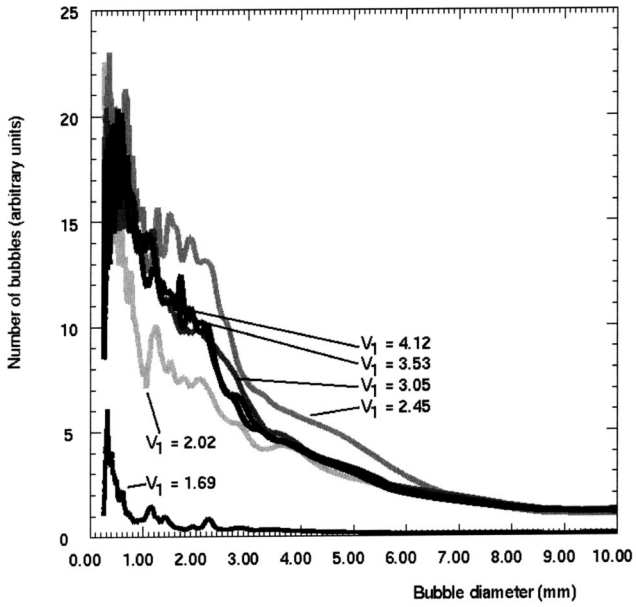

Fig. 10 Bubble-size spectra, jet height $x_1 = 100$ mm

Conclusions

Measurements in a large circular plunging jet flow show that there are three distinct regimes of air entrainment. These regimes are visually observable and boundaries between the second and third regimes are easily detectable acoustically. In the developing flow region, the spatial distributions of void fraction compares well with a solution of the advective diffusion equation (2) for all investigated flow conditions. Bubble count rate distributions exhibit a somehow different shape (Fig. 2) and there is a spatial offset in the peak of void fraction and bubble count, as with other two-dimensional plunging jet flows. The effects of the free-jet length were studied. The results showed an increased entrainment rate and increased dimensionless bubble count rate with increasing jet length for $x_1/d_1 \leqslant 12$.

Acoustic data reveal a bubble size population with a maximum probability around 1 mm in diameter, consistent with resistivity probe data. Since the acoustic bubble size measurements are measurements of true bubble volume, their distributions can be used to infer the presence of bubble breakup or coalescence. The results also suggest that, if the jet height is raised, the air bubble entrainment becomes insensitive to jet speed. The practical implication is

that in industrial systems, there is a threshold jet height above which pumping harder does not improve the aeration.

The acoustic technique can be accurately calibrated for a rapidly formed stream of bubbles precisely produced under laboratory conditions, [14]. The assessment of its accuracy is difficult in complex, high void-fraction flows, where the inherent bias towards large bubbles and acoustic interactions of bubble clouds can make interpretation of the signals in terms of fundamental theory problematic. Development of the acoustic technique as a semi-empirical signature method requires making comparative measurements using an alternative technique. The acoustic technique has so far yielded useful *relative* bubble size data, for example spatial differences in bubble size in a complex, high void-fraction flow. The present results suggest that an acoustic technique calibrated through detailed laboratory measurements can also yield useful, *absolute* data in high-void fraction flows. Moreover the robust acoustic sensor can then be used to make absolute measurements in hostile industrial or environmental flows where more delicate instruments are impractical.

Acknowledgments

The first writer acknowledges the assistance of his former students T. McGibbon, B. Bolden, T. Brattberg, and L. Toombes. He thanks Prof. C. J. Apelt, University of Queensland who supported this project since its beginning.

Nomenclature

C = air concentration defined as the volume of air per unit volume of air and water; it is also called void fraction
$C_{\max}$ = maximum void fraction in a cross section
D = bubble size (m)
D_1 = corrected mean bubble size (m)
D_{32} = Sauter mean diameter (m)
D_o = equilibrium (spherical) bubble diameter (m)
D_t = turbulent diffusivity (m^2/s)
$D^{\#}$ = dimensionless turbulent diffusivity: $D^{\#}=D_t/(V_1 r_1)$ for circular jet
d = jet diameter (m) measured perpendicular to the flow direction
d_1 = jet diameter (m) at the impact with the receiving pool of liquid
F = bubble count rate (Hz) defined as the number of detected bubbles per second
$F_{\max}$ = maximum bubble count rate (Hz) in a cross section
f = acoustic frequency (Hz)
g = gravity constant: $g=9.80\ m/s^2$ in Brisbane, Australia
I_o = modified Bessel function of the first kind of order zero
P = sound pressure (Pa)
P_∞ = absolute liquid pressure (Pa)
p = instantaneous sound pressure (Pa)
Q_{air} = air discharge (m^3/s)
Q_w = water discharge (m^3/s)
R = dimensionless radial distance: $R=2\,r/d_1$
r = radial distance (m) from the jet centerline
$r_{C_{\max}}$ = radial distance (m) where $C=C_{\max}$
$r_{F_{\max}}$ = radial distance (m) where $F=F_{\max}$
r_1 = jet radius (m) at impact
Tu = turbulence intensity defined as: $\text{Tu}=u'/V$
Tu_1 = turbulence intensity on the jet centerline measured at jet impact
Tu_o = turbulence intensity measured at jet nozzle
u = dimensionless variable
u' = root mean square of longitudinal component of turbulent velocity (m/s)
V = velocity (m/s)
V_1 = mean flow velocity (m/s) at jet impact
X = dimensionless longitudinal distance: $X=(x-x_1)/d_1$
x = distance along the flow direction (m) measured from the jet nozzle
x_1 = distance (m) between the jet nozzle and the impact flow conditions
γ = ratio of specific heats for the gas
θ, θ' = radial angular coordinate
ρ = liquid density (kg/m^3)
$\varnothing$ = diameter (m)

Subscripts

air = air flow
w = water flow
o = nozzle flow conditions
l = impact flow conditions

Appendix

Derivation of Bubble Sizes From Acoustic Data

Bubble Size Spectra. The relationship between bubble size and acoustic frequency is

$$f=\frac{1}{\pi D_o}\sqrt{\frac{3\gamma P_\infty}{\rho}} \tag{3}$$

where f is the frequency in Hz, P_∞ is the absolute liquid pressure, γ is the ratio of specific heats for the gas, ρ is the liquid density, and D_o is the equilibrium (spherical) bubble diameter, [12]. For these experiments, Eq. (3) becomes

$$f=\frac{6.58}{D_o}. \tag{4}$$

It is important to note that the acoustic frequency emitted by bubbles is essentially a function of the *cube root of bubble volume*. Severe distortions to the shape of the bubble (e.g., into a 4:1 ellipsoid) alter the frequency predicted by Eq. (4) by only 8%, [36]. Moreover bubbles tend to emit sounds when at their most spherical state, [14].

An acoustic spectrum of frequencies f may be inverted to give a spectrum of bubble sizes D_o. However, it is not correct to simply plot the sound power spectrum against the reciprocal of frequency, as Eq. (4) would suggest. Larger bubbles are louder and contribute more to the sound power. A spectral analysis would be biased unless a correction is introduced. Assumptions are required in comparing the relative excitation of bubbles. Pandit et al. [34] proposed a simple treatment. The instantaneous sound pressure produced by a single bubble, $p(t)$, is given by

$$p(t)^2=\frac{1}{f^2}\,\frac{3\gamma P_\infty^3}{4\pi^2\rho(\gamma(\gamma-1)r)^2}\,Y(t)^2 \tag{5}$$

where r is the distance from the bubble and the time-dependent factor $Y(t)$ is given by

$$Y(t)=\left(\frac{4}{3}-\gamma\right)\left(\frac{D_o}{D(t)}\right)^{3\gamma-1}+\frac{1}{3}\left(\frac{D_o}{D(t)}\right)^3 \tag{6}$$

for adiabatic compression of the bubble, where $D(t)$ is the instantaneous bubble diameter. This analysis does not, of course, consider the damping of the bubble, which gives rise to a broadening of the spectrum produced by any individual bubble. However, since time constants for the decay of a bubble pulse are significantly longer than the acoustic period, typically by a factor of 10–20 (e.g., typical pulses in Manasseh, [14,37]), the effect is not significant. For the simultaneous oscillations of n identical bubbles, the resultant summed sound pressure P, which would be measured by a hydrophone, is given by

$$P^2 = n\overline{p}^2 \tag{7}$$

where $\overline{p}$ is the rms value of $p(t)$. Using Eq. (5), this yields the corrected value of the frequency spectrum, N, as

$$N = P^2 f^2 K \tag{8}$$

where K is a function of the degree of excitation of the bubbles and of the distance between the bubbles and the hydrophone. Because sound power falls off as $1/r^2$, only bubbles close to the hydrophone contribute to the measured sound. The degree of excitation of the bubbles $(D_o/\overline{D})$ might differ with bubble sizes. In a plunging jet flow, it is likely that bubbles are excited both by their initial formation and by background turbulence, and it might be reasonable to assume $(D_o/\overline{D})$ being a constant. The overall factor K was assumed constant by Pandit et al. [34] and in the present work.

Bubble Size Distributions. The alternative ''first period'' method depends on an adjustable trigger level which will tend to bias the results towards larger bubbles, equivalent to the bias in the above spectrum-inversion approach. Assumptions are required to correct the distribution. Following the reasoning in Manasseh et al. [17], the use of a trigger means that only bubbles within a critical radius of the hydrophone get detected. This critical radius depends linearly on the bubble size. Assuming that the spatial distribution of bubbles is independent of their size, the number n_d of bubbles of a given size can be adjusted to the true number N_d, by equalizing the critical volumes:

$$N_d = n_d \left(\frac{D_{\text{ref}}}{D_o} \right)^3 \tag{9}$$

where D_{ref} is any reference bubble diameter. The distribution $N(D_o)$ is then normalized to ensure the total number of bubble counts is the same. The mean D_1 of a corrected distribution will generally be lower than the mean D_o of the raw distribution.

As noted above, in the plunging-jet context the pulse-damping time constant is likely to be an order of magnitude greater than the acoustic period, so spectral broadening is not likely to be significant. Nonetheless, it is worth noting that the use of the first period virtually eliminates effects of spectral broadening on the results.

In a complex bubbly flow, an additional phenomenon will result in a distortion of the measured bubble sizes away from the true sizes. It is well known that as bubbles are brought closer together, their acoustic emission frequency drops, [38,39]. The cloud of bubbles tends to behave as a continuum—one large composite bubble which has a lower frequency. In a flow where many bubbles are close together, the measured bubble sizes will be greater than the true sizes. This effect is not explicitly corrected for in the analyses presented in this paper. However, the underlying algorithm used to generate the bubble size distributions was introduced after noting that it gave more accurate results than conventional techniques when bubbles were closer together, [17]. The interaction effect is thus reduced, but cannot be eliminated entirely.

References

[1] Jameson, G. L., 1995, ''Bubbly Flows and the Plunging Jet Flotation Column,'' *Proceedings of 12th Australasian Fluid Mechanics Conference*, R. W. Bilger, ed., Sydney, Australia, **2**, pp. 735–742.

[2] Chanson, H., 1997, *Air Bubble Entrainment in Free-Surface Turbulent Shear Flows*, Academic Press, London.

[3] Kolani, A. R., Oguz, H. N., and Prosperetti, A., 1998, ''A New Aeration Device,'' *Proceedings ASME Fluids Eng. Summer Meeting*, June 21–25, Washington, D.C., **257**, pp. 111–145.

[4] Cummings, P. D., and Chanson, H., 1997, ''Air Entrainment in the Developing Flow Region of Plunging Jets. Part 1: Theoretical Development,'' ASME J. Fluids Eng., **119**(3), pp. 597–602.

[5] Cummings, P. D., and Chanson, H., 1997, ''Air Entrainment in the Developing Flow Region of Plunging Jets. Part 2: Experimental,'' ASME J. Fluids Eng., **119**(3), pp. 603–608.

[6] Brattberg, T., and Chanson, H., 1998, ''Air Entrapment and Air Bubble Dispersion at Two-Dimensional Plunging Water Jets,'' Chem. Eng. Sci., **53**(24), pp. 4113–4127; Errata: 1999, **54**(12), p. 1925.

[7] Bin, A. K., 1993, ''Gas Entrainment by Plunging Liquid Jets,'' Chem. Eng. Sci., **48**(21), pp. 3585–3630.

[8] Ervine, D. A., 1998, ''Air Entrainment in Hydraulic Structures: a Review,'' Proceedings of Institute of Civil Engineers, *Water, Maritime & Energy*, UK, **130**, pp. 142–153.

[9] Ervine, D. A., McKeogh, E. J., and Elsawy, E. M., 1980, ''Effect of Turbulence Intensity on the Rate of Air Entrainment by Plunging Water Jets,'' Proceedings of the Institute of Civil Engineering., Part 2, June, pp. 425–445.

[10] Cummings, P. D., and Chanson, H., 1999, ''An Experimental Study of Individual Air Bubble Entrainment at a Planar Plunging Jet,'' Chem. Eng. Res. Des., **77**(A2), pp. 159–164.

[11] Chanson, H., and Brattberg, T., 1998, ''Air Entrainment by Two-Dimensional Plunging Jets: The Impingement Region and the Very-Near Flow Field,'' *Proc. 1998 ASME Fluids Eng. Conf.*, FEDSM'98, Washington, DC, June 21–25, FEDSM98-4806.

[12] Minnaert, M., 1933, ''On Musical Air Bubbles and the Sound of Running Water,'' Philos. Mag., **16**, pp. 235–248.

[13] Leighton, T. G., 1994, *The Acoustic Bubble*, Academic Press, London.

[14] Manasseh, R., 1997, ''Acoustic Sizing of Bubbles at Moderate to High Bubbling Rates,'' *Proc. 4th World Conference on Experimental Heat Transfer, Fluid Mechanics and Thermodynamics*, Brussels, 2–6, June.

[15] Boyd, J. W. R., and Varley, J., 2001, ''The Uses of Passive Measurement of Acoustic Emissions From Chemical Engineering Processes,'' Chem. Eng. Sci., **56**, pp. 1749–1767.

[16] Manasseh, R., and Chanson, H., 2001, ''Void-Fraction and Acoustic Characteristics of Gas Bubbles Entrained by a Circular Plunging Jet,'' *Proc. 4th Intl Conf. Multiphase Flow*, ICMF'01, E. E. Michaelides, ed., New Orleans, LA.

[17] Manasseh, R., LaFontaine, R. F., Davy, J., Shepherd, I. C., and Zhu, Y., 2001, ''Passive Acoustic Bubble Sizing in Sparged Systems,'' Exp. Fluids, **30**(6), pp. 672–682.

[18] Esslingen, 1984, ''Scale Effects in Modelling Hydraulic Structures,'' *Proceedings of the International Symposium on Scale Effects in Modelling Hydraulic Structures*, H. Kobus, ed., IAHR, Esslingen, Germany.

[19] Wood, I. R., 1991, ''Air Entrainment in Free-Surface Flows,'' *IAHR Hydraulic Structures Design Manual No. 4, Hydraulic Design Considerations*, Balkema, Rotterdam.

[20] McKeogh, E. J., 1978, ''A Study of Air Entrainment Using Plunging Water Jets,'' Ph.D. thesis, Queen's University of Belfast, UK.

[21] El-Hammoumi, M., 1994, ''Entraînement d'Air par Jet Plongeant Vertical. Application aux Becs de Remplissage Pour le Dosage Pondéral,'' Ph.D. thesis, INPG, Grenoble, France (in French).

[22] Oguz, H. N., 1998, ''The Role of Surface Disturbances in the Entrainment of Bubbles by a Liquid Jet,'' J. Fluid Mech., **372**, pp. 189–212.

[23] Zhu, Y., Oguz, H., and Prosperetti, A., 2000, ''On the Mechanism of Air Entrainment by Liquid Jets at a Free Surface,'' J. Fluid Mech., **404**, pp. 151–177.

[24] Lunde, K., and Perkins, R. J., 1996, ''A Method for the Detailed Study of Bubble Motion and Deformation,'' *Multiphase Flow 1995, Proceedings of the 2nd Int. Conference on Multiphase Flow*, A. Serizawa, T. Fukano, and J. Bataille, eds., pp. 395–405.

[25] Yoshida, S., Manasseh, R., and Kajio, N., 1998, ''The Structure of Bubble Trajectories Under Continuous Sparging Conditions,'' *Proceedings, 3rd International Conference on Multiphase Flow*, Lyon, France.

[26] Manasseh, R., Yoshida, S., and Kajio, N., 1998, ''Bubble Trajectory Bifurcations in Cross Flow,'' *Proceedings, 13th Australasian Fluid Mechanics Conference*, Monash University, Melbourne, Dec. 13–18, pp. 1013–1018.

[27] Bonetto, F., and Lahey, R. T., Jr., 1993, ''An Experimental Study on Air Carryunder due to a Plunging Liquid Jet,'' Int. J. Multiphase Flow, **19**(2), pp. 281–294.

[28] Detsch, R. M., and Sharma, R. N., 1990, ''The Critical Angle for Gas Bubble Entrainment by Plunging Liquid Jets,'' Chem. Eng. J., **44**, pp. 157–166.

[29] McKeogh, E. J., and Ervine, D. A., 1981, ''Air Entrainment Rate and Diffusion Pattern of Plunging Liquid Jets,'' Chem. Eng. Sci., **36**, pp. 1161–1172.

[30] Moursali, E., Marie, J. L., and Bataille, J., 1995, ''An Upward Turbulent Bubbly Boundary Layer Along a Vertical Flat Plate,'' Int. J. Multiphase Flow, **21**(1), pp. 107–117.

[31] Chanson, H., 2002, ''Air-Water Flow Measurements With Intrusive Phase-Detection Probes. Can we Improve Their Interpretation?'' J. Hydraul. Eng., **128**(3), pp. 252–255.

[32] Van de Sande, E., and Smith, J. M., 1973, ''Surface Entrainment of Air by High Velocity Water Jets,'' Chem. Eng. Sci., **28**, pp. 1161–1168.

[33] Clanet, C., and Lasheras, J. C., 1998, ''Depth of Penetration of Bubbles Entrained by a Plunging Water Jet,'' Phys. Fluids, **9**(7), pp. 1864–1866.

[34] Pandit, A. B., Varley, J., Thorpe, R. B., and Davidson, J. F., 1992, ''Measurement of Bubble Size Distribution: An Acoustic Technique,'' Chem. Eng. Sci., **47**(5), pp. 1079–1089.

[35] Cummings, P. D., and Chanson, H., 1998, ''Individual Air Bubble Entrapment at a Planar Plunging Jet With Near-Inception Flow Conditions,'' *Proceedings, 13th Australasian Fluid Mechanics Conference*, Monash University, Melbourne, Australia, Dec. 13–18.

[36] Strasberg, M., 1953, ''The Pulsation Frequency of Nonspherical Gas Bubbles in Liquid,'' J. Acoust. Soc. Am., **25**, pp. 536–537.

[37] Manasseh, R., Yoshida, S., and Rudman, M., 1998, ''Bubble Formation Processes and Bubble Acoustic Signals,'' *Proc 3rd Intl. Conf. Multiphase Flow*, ICMF98, J. Bataille, ed., Lyon, France.
[38] Lu, N. Q., Prosperetti, A., and Yoon, S. W., 1990, ''Underwater Noise Emissions From Bubble Clouds,'' IEEE J. Ocean. Eng., **15**(4), pp. 275–281.
[39] Nicholas, M., Roy, R. A., Crum, L. A., Oguz, H., and Prosperetti, A., 1994, ''Sound Emissions by a Laboratory Bubble Cloud,'' J. Acoust. Soc. Am., **95**(6), pp. 3171–3182.
[40] Lin, T. J., and Donnelly, H. G., 1966, ''Gas Bubble Entrainment by Plunging Laminar Liquid Jets,'' AIChE J., **12**(3), pp. 563–571.
[41] Van de Donk, J., 1981, ''Water Aeration With Plunging Jets,'' Ph.D. thesis, TH Delft, The Netherlands.